Rapid Communications

Theoretical determination of hydrodynamic window in monolayer and bilayer graphene from scattering rates

Derek Y. H. Ho,[1] Indra Yudhistira,[1,2] Nilotpal Chakraborty,[3] and Shaffique Adam[1,2,3,*]

[1]*Centre for Advanced 2D Materials and Graphene Research Centre, National University of Singapore, 6 Science Drive 2, 117546 Singapore*

[2]*Department of Physics, National University of Singapore, 2 Science Drive 3, 117551 Singapore*

[3]*Yale-NUS College, 16 College Avenue West, 138614 Singapore*

(Received 12 December 2017; published 22 March 2018)

Electrons behave like a classical fluid with a momentum distribution function that varies slowly in space and time when the quantum-mechanical carrier-carrier scattering dominates over all other scattering processes. Recent experiments in monolayer and bilayer graphene have reported signatures of such hydrodynamic electron behavior in ultraclean devices. In this theoretical work, starting from a microscopic treatment of electron-electron, electron-phonon, and electron-impurity interactions within the random phase approximation, we demonstrate that monolayer and bilayer graphene both host two different hydrodynamic regimes. We predict that the hydrodynamic window in bilayer graphene is stronger than in monolayer graphene, and has a characteristic "v shape" as opposed to a "lung shape." Finally, we collapse experimental data onto a universal disorder-limited theory, demonstrating that the observed violation of the Wiedemann-Franz law in monolayers occurs in a regime dominated by impurity-induced electron-hole puddles.

DOI: 10.1103/PhysRevB.97.121404

For most metals, electronlike quasiparticles with Fermi-Dirac statistics move ballistically like classical billiard balls between collision centers, while the scattering cross sections during the collisions are treated quantum mechanically. These properties are captured by solving the Boltzmann equation for the semiclassical distribution function. In the unusual case where the carrier-carrier scattering dominates over all other kinds of scattering, a coarse-graining procedure transforms the Boltzmann equation into hydrodynamic quantities governed by classical fluid mechanics [1]. Various proposals for effects that are peculiar for electrons can manifest themselves in such a hydrodynamic regime including a nonmonotonic temperature dependence of resistivity that marks the transition from boundary-limited to viscous flow [2], an electron Bernoulli effect [3], spontaneous excitation of plasma oscillations [4], signatures of electron viscosity in magnetotransport [5,6], and faster than ballistic electron transport [7].

In spite of more than 50 years of theorizing about electron hydrodynamics, experimental observation has been sparse and disputed (see, e.g., Ref. [8]). The reason is that in many experimental configurations electron-impurity scattering dominates at low temperatures while electron-phonon scattering dominates at high temperatures providing a small window in temperature (if any) for observing such electron hydrodynamics. The experimental situation changed recently with reports of charge carriers behaving hydrodynamically in monolayer [9,10] and bilayer graphene [9,11] from groups at Harvard, Manchester, and Geneva (see also Ref. [12] that reported a large viscous contribution to the resistance of palladium cobaltate).

It is important to note that gapless (or narrow band-gap) materials support two very different types of hydrodynamic regimes depending on whether the temperature is larger or smaller than the Fermi energy. At low temperature, only one carrier contributes to the hydrodynamic Fermi liquid and the transport can be described using a single macroscopic charge current evolving under the standard Navier-Stokes equation [13]. This is in contrast to high temperature, where electron and hole densities are comparable giving rise to a hydrodynamic plasma that involves three coupled macroscopic currents [14,15]. While the Manchester and Harvard groups used samples of comparable quality, the former observed only single fluid hydrodynamics, and the latter only the coupled plasma regime.

In this Rapid Communication, we show that for monolayer and bilayer graphene, a large and robust hydrodynamic window exists over a wide range of carrier densities and temperatures supporting both the plasma and single-carrier hydrodynamic regimes (for monolayer, this requires impurity concentrations lower than $\sim 10^{11}$ cm^{-2}, while no such constraint applies for bilayers). We predict very different hydrodynamic windows for monolayer and bilayer graphene due to a subtle competition between different scattering mechanisms. The difference between the experiments is that the negative nonlocal resistance measurement at Manchester (which is a proxy for viscous backflow) is observed only in the single-carrier regime, while the violation of the Wiedmann-Franz law seen at Harvard occurs in the electron-hole plasma regime. We find curiously that the largest violations of the Wiedemann-Franz law occurs in a regime where the electrical conductivity is well described by a disorder-limited theory. Our calculation of the interaction-limited quasiparticle lifetime in bilayer graphene shows a universal scaling collapse in agreement with the observation in Geneva of electron-hole scattering limited transport [11].

Our main goal is a careful comparison of the various scattering mechanisms in order to decide when the electronic

*shaffique.adam@yale-nus.edu.sg

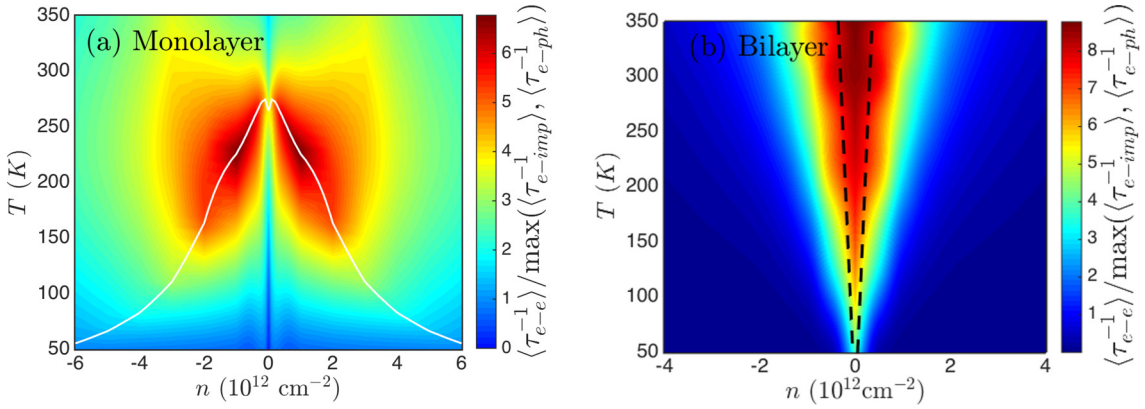

FIG. 1. Hydrodynamic window in (a) monolayer graphene and (b) bilayer graphene determined by comparing the carrier-carrier scattering rate to that of impurities and phonons. For monolayer graphene the lung shape is determined by the competition between electron-impurity scattering that dominates at low temperature and carrier density, and electron-phonon scattering that dominates at high temperature and density. The solid white line traces the points where these two contributions are equal. For bilayer graphene, we find that the electron-electron scattering is much stronger than in monolayer graphene at the Dirac point, but drops off faster as a function of carrier density. This yields the v shape where electron-electron interactions dominate over electron-phonon interactions at low carrier density, but are weaker at higher carrier density. The dashed black lines show crossover from the plasma regime that comprises thermal occupation of both electrons and holes to the single-carrier regime. Regardless of the amount of disorder, at sufficiently high temperature, bilayer graphene supports both types of hydrodymamics. Impurity concentration $n_{\text{imp}} = 9\times10^9$ cm^{-2} is used for both panels.

system is described by the hydrodynamic equations. We therefore look at the contribution to the quasiparticle lifetime $\tau(\varepsilon) = \hbar/2\,\text{Im}[\Sigma(\varepsilon)]$, where $\Sigma(\varepsilon)$ is the corresponding self-energy calculated within the random phase approximation (RPA) for that scattering process. At a given carrier density n and temperature T, the contribution of a given scattering mechanism to the quasiparticle lifetime is obtained by thermal averaging [16]

$$\langle\tau^{-1}\rangle = \frac{\int_{-\infty}^{\infty} d\varepsilon|\varepsilon|\frac{\partial n_F(\varepsilon-\mu)}{\partial\varepsilon}\tau^{-1}(\varepsilon)}{\int_{-\infty}^{\infty} d\varepsilon|\varepsilon|\frac{\partial n_F(\varepsilon-\mu)}{\partial\varepsilon}}, \tag{1}$$

where n_F is the Fermi-Dirac distribution. Different ways of performing this average give quantitatively different but qualitatively similar results; we choose this form of thermal averaging to be consistent with Ref. [16]. The chemical potential μ is found by solving $n = n_e - n_h$ [17]. For monolayer graphene, the self-energy $\Sigma^{\text{RPA}}(\varepsilon)$ for various scattering mechanisms is known in the literature [see, e.g., Ref. [18] for electron-electron (e-e) scattering, Ref. [19] for electron-impurity (e-imp) scattering, and Ref. [20] for electron-phonon (e-ph) scattering]; however, here we do thermal averaging for the e-ph and e-imp contributions. For bilayer (discussed in more detail below), we calculate the self-energy for the e-e scattering mechanism within the RPA, in addition to performing the thermal average for e-ph and e-imp contributions. In the plasma regime where there are both electron and hole carriers, we count all appropriate channels, i.e., $\langle\tau_{cc}^{-1}\rangle = \langle\tau_{ee}^{-1}\rangle + \langle\tau_{eh}^{-1}\rangle + \langle\tau_{hh}^{-1}\rangle$ (which for notational simplicity, we generically call $\langle\tau_{ee}^{-1}\rangle$ for the remainder of this Rapid Communication). The above procedure determines $\langle\tau_{ee}^{-1}\rangle$, $\langle\tau_{\text{e-imp}}^{-1}\rangle$, and $\langle\tau_{\text{e-ph}}^{-1}\rangle$. We then identify the hydrodynamic regime as when $\langle\tau_{ee}^{-1}\rangle > \langle\tau_{\text{e-imp}}^{-1}\rangle, \langle\tau_{\text{e-ph}}^{-1}\rangle$.

Our main results can be seen in Fig. 1. The color axis shows the ratio of the e-e scattering rate to maximum of the other scattering rates (e-imp and e-ph). Dark red represents the regions where collisions between carriers dominate the quasiparticle lifetime. The most striking feature is that the window for hydrodynamics is "lung shaped" in monolayer graphene, while it is "v shaped" in bilayer. The absolute magnitude of the ratio is also larger in bilayer graphene, implying that hydrodynamic effects are stronger. We now describe some features of the hydrodynamic window. For monolayer, the e-imp scattering rate diverges at $n \to 0$ and $T \to 0$ which explains the reduced hydrodynamic window both close to the Dirac point and at low temperature (this divergence also causes electron-hole puddles which we discuss later). The white line marks the points in the (n,T) phase space where $\tau_{\text{e-imp}} = \tau_{\text{e-ph}}$ implying that the crossover to the hydrodynamic window below this line is set entirely by the competition of e-e and e-imp scattering. Above the white line (i.e., at higher density and temperature) the emergence of hydrodynamics is determined only by the competition between e-ph and e-e interactions. The suppression of the window at the Dirac point above the white line is caused by the transverse optical mode at the Brillouin zone boundary, commonly referred to as the A_1' mode [20]. At any given temperature, the hydrodynamic window eventually closes with increasing density since both e-e scattering decreases (because of Pauli blocking and enhanced screening) and acoustic phonon scattering increases. The lung shape arises because the A_1' phonons peak at the Dirac point and decrease sharply with density, while the acoustic phonons, which are minimal at the Dirac point, increase with density. Bilayer graphene has a very different hydrodynamic window due to the stronger e-e scattering and weaker e-imp scattering. Regardless of the amount of disorder, at sufficiently high temperature, e-imp scattering contributes negligibly to the quasiparticle lifetime, e.g., for an estimated $n_{\text{imp}} = 9\times10^9$ cm^{-2} for bilayer graphene on h-BN, this is already the case at $T \gtrsim 10$ K. Unlike the monolayer case, there is no high-temperature cutoff to the hydrodynamic window because there is no analog to the A_1' phonon mode [21]. At the Dirac point, we find that the acoustic e-ph and e-e scattering

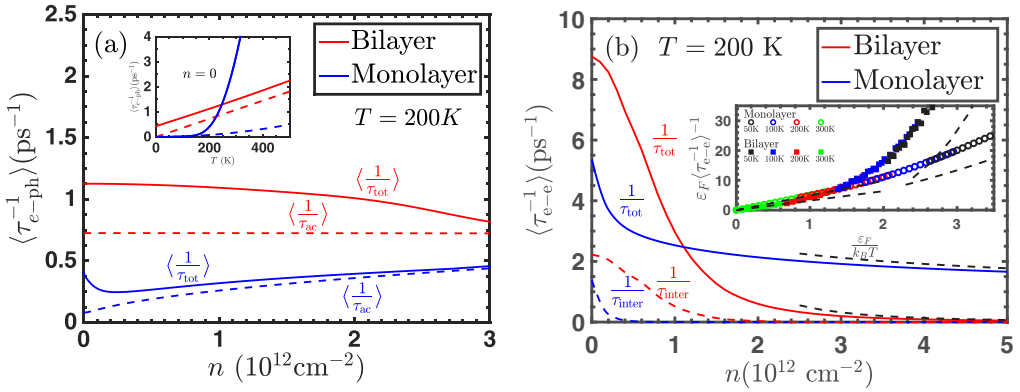

FIG. 2. (a) Electron-phonon scattering. Monolayer graphene is mostly acoustic phonons (dashed line) at high density and A_1' optical phonon at very low density. For bilayer, both acoustic (dashed line) and surface polar phonons contribute to the total $\tau_{\text{e-ph}}$ (solid lines). Inset shows results at charge neutrality for the total phonon scattering rate (solid lines) and the acoustic phonon contribution (dashed lines). For monolayer graphene, we use $\alpha = 0.57$. (b) Electron-electron scattering follows a universal scaling function. Solid (dashed) lines in the main panel represent the total (interband) e-e scattering rate. Dashed black lines represent high-density asymptotes of the universal scaling function. Inset shows the collapse of $\epsilon_F \langle \tau_{ee}^{-1} \rangle^{-1}$ as a function of single parameter $\varepsilon_F / k_B T$ for different temperatures. For $\varepsilon_F \ll k_B T$, the scaling function is linear for both monolayer and bilayer graphene while for $\varepsilon_F \gg k_B T$ (beyond the range shown in the inset) bilayer has a stronger x^4 power law compared to the $x^{\sim 2}$ for monolayer.

rates increase linearly with temperature, but the coefficient of the e-e scattering rate is much stronger. Hence, we find the hydrodynamic regime in bilayer graphene for the full range of parameters explored in Fig. 1. In addition, as indicated by the dashed lines in Fig. 1(b) both the plasma hydrodynamic fluid and the single-carrier hydrodynamics always exist in bilayer graphene. The v shape arises because although e-e scattering peaks at the Dirac point, it decays strongly as a (universal) function of $\varepsilon_F / k_B T$, implying a larger window at higher temperatures.

We now describe our calculations in more detail. For monolayer graphene, the e-ph scattering is dominated by the in-plane longitudinal and transverse acoustic modes [we use the expressions from Ref. [20], but convert the transport scattering rates to quasiparticle rates by removing the $(1 - \cos\theta)$ Boltzmann factor before performing the thermal average using Eq. (1)]. Our results are displayed in Fig. 2(a) (blue curves). We note that at fixed temperature, electron scattering with A_1' modes (acoustic modes) decreases (increases) with density giving rise to a nonmonotonic e-ph scattering rate as a function of density. For bilayer the dominant phonons are the acoustic [21] and surface polar [22] modes, which we suitably adapt before doing the thermal average for each mode separately and adding the rates together to obtain the results in Fig. 2(a) (red curves). We note that the total e-ph rate is an almost constant function of density, and increases linearly in T. The weak temperature dependence of bilayer phonons compared to monolayer phonons [see inset to Fig. 2(a)] illustrates why there is no high-temperature cutoff of the bilayer hydrodynamic regime.

Since we find no calculation in the literature of the quasiparticle lifetime in bilayer graphene due to e-e scattering, we calculate it starting from the RPA approximation for the self-energy [18]

$$\text{Im}[\Sigma_\lambda(\boldsymbol{k},\omega)] = -\int \frac{d^2\boldsymbol{q}}{(2\pi)^2} \sum_{\lambda'} \text{Im}\left[\frac{V(q)}{\epsilon(q,\omega - \varepsilon_{\boldsymbol{k}-\boldsymbol{q},\lambda'} + \mu, T)}\right] \mathcal{F}_{\lambda\lambda'}(\theta_{\boldsymbol{k},\boldsymbol{k}-\boldsymbol{q}}) [n_{\text{B}}(\omega - \varepsilon_{\boldsymbol{k}-\boldsymbol{q},\lambda'} + \mu) + n_{\text{F}}(-\varepsilon_{\boldsymbol{k}-\boldsymbol{q},\lambda'} + \mu)], \quad (2)$$

where $V(q) = 2\pi e^2/(\kappa q)$ is the Coulomb potential, $n_{\text{B/F}}(x) \equiv 1/[\exp(\beta x) \mp 1]$ the Bose (Fermi) distribution function, λ, λ' are band indices ($\pm$ denote the conduction and valence bands), $\mathcal{F}_{\lambda\lambda'}(\varphi) = (1 + \lambda\lambda' \cos 2\varphi)/2$ the chirality factor, and φ the scattering angle. $\varepsilon_{\boldsymbol{k},\lambda} = \lambda \hbar^2 k^2/(2m^\star)$ are parabolic-band single-particle energies and $\epsilon(q,\omega,T) \equiv 1 - V(q)\Pi(q,\omega,T)$ refers to the dynamical RPA dielectric function first calculated in Ref. [23]. We show in Fig. 2(b) our calculations of $\langle \tau_{\text{ee}}^{-1} \rangle$ as a function of density for both monolayer and bilayer graphene. The primary difference between the two is that for bilayer graphene the scattering rate drops sharply as a function of density, whereas for monolayers it drops much more slowly. Remarkably, we show that after thermal averaging, $\varepsilon_{\text{F}} \langle \tau_{ee}^{-1} \rangle^{-1}$ for both monolayer (m) and bilayer (b) graphene is given by a one-parameter function $F_{m,b}(\varepsilon_F / k_B T)$ [see inset to Fig. 2(b)]. For monolayers, this is an exact result for fixed α, while for bilayers, the scaling requires $T \lesssim 2\alpha^2 (m^* v_F^2) \approx 1700$ K (here α and v_F are the monolayer fine-structure constant and Fermi velocity, respectively, and m^* the bilayer effective mass). This is an especially useful result given that three numerical integrals are required to evaluate e-e scattering at each density and temperature. We find numerically that the scaling function obeys the following asymptotes: At low density or high temperature, $F_m(x \ll 1) \sim 4.9x$ and $F_b(x \ll 1) \sim 3.2x$, while in the opposite limit $F_m(x \gg 1) \sim 2.1x^{1.7}$ and $F_b(x \gg 1) \sim 0.4x^4$. Our theoretical finding that the e-e scattering rate at the Dirac point for bilayer graphene is linear in temperature, i.e., $\hbar \langle \tau_{ee}^{-1} \rangle = 0.3 k_B T$, was recently observed experimentally [11].

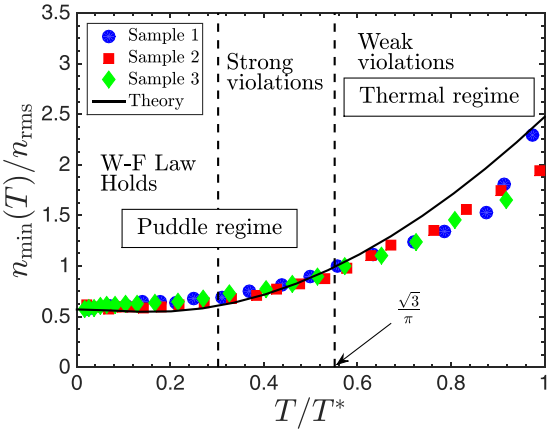

FIG. 3. Collapse of $n_{\min}/n_{\rm rms}$ as a function of the scaled temperature T/T^* where $k_B T^* = \varepsilon_F(n = n_{\rm rms})$. Symbols correspond to data extracted from the experiment of Ref. [10] and the solid line corresponds to the universal disorder-limited theory. The second dashed line marks the temperature when thermally excited carrier density equals the disorder-induced electron-hole puddle density.

So far we have ignored the role of electron-hole puddles. Reference [17] showed that when impurities were responsible for both scattering electrons and for inducing density fluctuations, the temperature-dependent charge conductivity followed a one-parameter scaling. We show the scaling as follows: $n_{\min}(T)$, a quantity defined in the experimental work, is determined by extrapolating a linear fit of $\log\sigma(n,T)$ down to the minimum conductivity. The analogous theoretical quantity is $n_{\rm rms}$ where Ref. [24] showed that $n_{\min}(T=0) = n_{\rm rms}/\sqrt{3} = (k_B T^*/\hbar v_F)^2/\pi$, where T^* is a corresponding disorder temperature scale. Figure 3 shows the collapse of the experimental $n_{\min}/n_{\rm rms}$ as a function of experimental T/T^* for the three samples reported in Ref. [10]. This implies that for the experiment, the charge transport is limited by the same mechanism responsible for the puddles.

This universal disorder-limited curve may be calculated theoretically. We obtain the e-imp-limited RPA-effective medium conductivity [25,26] as a function of n and T and extract the effective density at Dirac point $n_{\min}(T)$ using the same procedure described above. Our theory shows excellent agreement with experiment over a wide range, with weak deviations occurring only at high temperatures $T/T^* \gtrsim 0.55$. [This is when thermally excited carriers outnumber the puddle carriers induced by impurities, i.e., $n_e(0,T_c) + n_h(0,T_c) = n_{\rm rms}$, where $T_c = \sqrt{3}T^*/\pi \approx 0.55T^*$.] This confirms that charge conductivity at temperatures at which the largest violations of the Wiedemann-Franz law were observed is completely understood within a model considering only charged impurity scattering.

Our results allow us to speculate regarding the recent experiments. The Harvard experiments observed a strong violation of the Wiedemann-Franz law (with Lorenz ratios as high as 22) in a temperature range about a factor of 2 lower than when we might expect the system to be hydrodynamic. This was interpreted as a signature of the theoretically predicted Dirac fluid [27,28] where the thermal conductivity diverges and the electrical conductivity approaches a universal minimum value of $\sigma_0 = 4/\pi\, e^2/h$. However, this would also imply a nonmonotonic $\sigma_{\min}(T)$ as the plasma evolved from the disorder-dominated puddle regime (where $\sigma_{\min}$ increases with T) to the ideal Dirac fluid regime (where $\sigma_{\min} = \sigma_0$ remains constant with increasing T). Not only does the experimental electrical conductivity increase monotonically, but its value quantitatively agrees with the disorder-limited theory in which the absolute value of the conductivity is $\sim 10\sigma_0$. This agreement allows us to conclude that the violations of the Wiedemann-Franz law seen in experiment arise from the thermal rather than the charge transport sector (where this enhancement occurs because in the plasma regime carrier-carrier collisions are unable to relax thermal currents). Our calculations suggest that if one moves out of the plasma regime (i.e., within the "lung region" in Fig. 1), then there should be weak violation of the Wiedemann-Franz law with a *reduced* Lorenz ratio, because in the single-carrier collision-limited regime charge currents are almost completely unaffected by carrier-carrier collisions, while thermal currents can be strongly degraded [29,30]. This prediction is consistent with the Harvard experiment. Our results show that the hydrodynamic regime is stronger in bilayer graphene, becoming increasingly stronger at higher temperature. However, we emphasize that deciding when the system is hydrodynamic and when there is a violation of the Wiedemann-Franz law are two separate questions, and one can have one without the other [31]. In particular, the argument for the conservation of thermal conductivity at the Dirac point in monolayer graphene does not hold in bilayer graphene. So although bilayer graphene is *more* hydrodynamic than monolayer graphene, this does not guarantee strong violation in the Wiedemann-Franz law.

Turning to the Manchester experiments, there is good qualitative agreement with the shapes of hydrodynamic window shown in Fig. 1 (i.e., a lung for monolayer and a v shape for bilayer) and those seen experimentally. We note that no whirlpools were observed in the plasma hydrodynamic regime [dashed lines in Fig. 1(b)], possibly because of the presence of electrons and holes moving in opposite directions. In particular, our finding that the monolayer hydrodynamic window is cut off by phonons at high temperature, but not in bilayer graphene is consistent with the experimental observations. The details of the lung-shape in monolayer graphene is somewhat different, but our conclusion that the low-temperature boundary is set by impurities and the high-temperature boundary is set by phonons should remain robust regardless of the impurity and phonon models used (e.g., it seems that the ratio of A_1' to acoustic phonon modes is weaker in the experiment than in the best available models [20]). Although the bilayer e-e scattering rate is larger at higher temperature, giving a wider window in carrier density where hydrodynamics can be observed, the viscosity is lower at higher temperature making the whirlpools more difficult to observe. Again, just like for the violation of the Widemann-Franz law, there is not a perfect correlation between the hydrodynamic regime and observations of negative vicinity resistance.

Note added. Recently, we noticed on arXiv a useful review article on graphene hydrodynamics [32] that provides a broader context for the relevance of our work.

It is a pleasure to thank Sankar Das Sarma, Matthew Foster, Ben Yu-Kuang Hu, Euyheon Hwang, Philip Kim, Andrew Lucas, Boris Narozhny, Marco Polini, Subir Sachdev, Thibault

Sohier, and Giovanni Vignale for valuable discussions, and acknowledge the support of the National Research Foundation of Singapore under its Fellowship program (NRF-NRFF2012-01) and Singapore Ministry of Education AcRF Tier 2 (MOE2017-T2-1-130). We also acknowledge use of the dedicated research computing resources at CA2DM.

[1] E. M. Lifshitz and L. P. Pitaevski, *Physical Kinetics*, Landau and Lifshitz, Course of Theoretical Physics Vol. 10 (Pergamon Press, Oxford, 1981).
[2] R. N. Gurzhi, Sov. Phys. Usp. **11**, 255 (1968).
[3] A. O. Govorov and J. J. Heremans, Phys. Rev. Lett. **92**, 026803 (2004).
[4] M. Dyakonov and M. Shur, Phys. Rev. Lett. **71**, 2465 (1993).
[5] J. E. Avron, R. Seiler, and P. G. Zograf, Phys. Rev. Lett. **75**, 697 (1995).
[6] P. S. Alekseev, Phys. Rev. Lett. **117**, 166601 (2016).
[7] H. Guo, E. Ilseven, G. Falkovich, and L. S. Levitov, Proc. Natl. Acad. Sci. USA **114**, 3068 (2017).
[8] M. J. M. de Jong and L. W. Molenkamp, Phys. Rev. B **51**, 13389 (1995).
[9] D. A. Bandurin, I. Torre, R. K. Kumar, M. B. Shalom, A. Tomadin, A. Principi, G. H. Auton, E. Khestanova, K. S. Novoselov, I. V. Grigorieva, L. A. Ponomarenko, A. K. Geim, and M. Polini, Science **351**, 1055 (2016).
[10] J. Crossno, J. K. Shi, K. Wang, X. Liu, A. Harzheim, A. Lucas, S. Sachdev, P. Kim, T. Taniguchi, K. Watanabe, T. A. Ohki, and K. C. Fong, Science **351**, 1058 (2016).
[11] Y. Nam, D.-K. Ki, D. Soler-Delgado, and A. F. Morpurgo, Nat. Phys. **13**, 1207 (2017).
[12] P. J. W. Moll, P. Kushwaha, N. Nandi, B. Schmidt, and A. P. Mackenzie, Science **351**, 1061 (2016).
[13] I. Torre, A. Tomadin, A. K. Geim, and M. Polini, Phys. Rev. B **92**, 165433 (2015).
[14] B. N. Narozhny, I. V. Gornyi, M. Titov, M. Schütt, and A. D. Mirlin, Phys. Rev. B **91**, 035414 (2015).
[15] A. Lucas, J. Crossno, K. C. Fong, P. Kim, and S. Sachdev, Phys. Rev. B **93**, 075426 (2016).
[16] M. Schütt, P. M. Ostrovsky, I. V. Gornyi, and A. D. Mirlin, Phys. Rev. B **83**, 155441 (2011).
[17] S. Adam and M. D. Stiles, Phys. Rev. B **82**, 075423 (2010).
[18] M. Polini and G. Vignale, in *No-Nonsense Physicist: An Overview of Gabriele Giuliani's Work and Life*, edited by M. Polini, G. Vignale, V. Pellegrini, and J. K. Jain (Scuola Normale Superiore, Pisa, 2016).
[19] E. H. Hwang and S. Das Sarma, Phys. Rev. B **77**, 195412 (2008).
[20] T. Sohier, M. Calandra, C.-H. Park, N. Bonini, N. Marzari, and F. Mauri, Phys. Rev. B **90**, 125414 (2014).
[21] K. M. Borysenko, J. T. Mullen, X. Li, Y. G. Semenov, J. M. Zavada, M. B. Nardelli, and K. W. Kim, Phys. Rev. B **83**, 161402 (2011).
[22] X. Li, K. M. Borysenko, M. B. Nardelli, and K. W. Kim, Phys. Rev. B **84**, 195453 (2011).
[23] E. H. Hwang, R. Sensarma, and S. Das Sarma, Phys. Rev. B **84**, 245441 (2011).
[24] S. Adam, E. H. Hwang, V. M. Galitski, and S. Das Sarma, Proc. Natl. Acad. Sci. USA **104**, 18392 (2007).
[25] E. H. Hwang and S. Das Sarma, Phys. Rev. B **79**, 165404 (2009).
[26] E. Rossi, S. Adam, and S. Das Sarma, Phys. Rev. B **79**, 245423 (2009).
[27] L. Fritz, J. Schmalian, M. Müller, and S. Sachdev, Phys. Rev. B **78**, 085416 (2008).
[28] M. Müller, L. Fritz, and S. Sachdev, Phys. Rev. B **78**, 115406 (2008).
[29] A. Principi and G. Vignale, Phys. Rev. Lett. **115**, 056603 (2015).
[30] S. A. Hartnoll, P. K. Kovtun, M. Müller, and S. Sachdev, Phys. Rev. B **76**, 144502 (2007).
[31] H.-Y. Xie and M. S. Foster, Phys. Rev. B **93**, 195103 (2016).
[32] A. Lucas and K. C. Fong, J. Phys.: Condens. Matter **30**, 053001 (2018).